Alternative Design Approach for Ship Damage Stability Enhancement based on Crashworthiness

Hongseok Bae[1,2], **Dracos Vassalos**[1], **Evangelos Boulougouris**[1]

ABSTRACT

This paper focuses on the direct assessment of crashworthiness for ship collisions. A systematic methodology for quantitive risk analysis is being proposed to enhance damage survivability cost-effectively through crashworthy designs. The latter is used as risk control options for prevention or mitigation purposes from flooding risks within the current IMO framework.

KEY WORDS

Damage stability; Alternative design; Crashworthiness; ship collision; risk control option; passenger ship; crashworthy design

1 INTRODUCTION

Since *the Titanic* tragedy in 1912, international regulatory frameworks, especially for damage stability, have continuously evolved from the deterministic method to the probabilistic approach, tightening up the requirements to protect persons on board and enhance ship survivability. Nevertheless, many accidents, such as collisions and groundings, are still taking place, leading to losses of many lives and property even these days. Especially passenger ships carrying a number of persons face higher risks than other vessels from a single accident. However, it is true that the current SOLAS framework for damage stability of passenger ships (i.e. Subdivision Attained Index = $\sum p - factor \times s - factor$) cannot fully control or mitigate these risks due to the nature of the current SOLAS regulatory framework. Firstly, the damage occurrence probability (p-factor) defined in current probabilistic regulations is based on the accident statistics of all types of vessels, especially cargo ships, which were established from the EU-funded project HARDER (2000-2003), and it has not been changed yet for two decades. Secondly, it is basically assumed that flooding will take place for each damage case, disregarding the collision resistance of ship structures. Therefore, it completely ignores and cannot evaluate contributions of innovative structural designs, such as new structural arrangements and crashworthy material application, as the current regulatory concept treats them the same as a "typical structure". Additionally, predetermined breach distributions (p-factors) cause biased damage stability solutions solely focusing on ship survival improvement (s-factor), disregarding ship individual operating characteristics such as operating area and profiles. To address these problems in SOLAS regulations, Vassalos et al. (2022) suggested either applying the actual breach distribution to passenger ships in question based on the passenger ship accident statistics or performing a direct assessment with crashworthiness analysis using collision simulations.

In particular, for the latter, Germanischer Lloyd (IMO, 2003, Zhang et al., 2004) have introduced a direct analysis as an approval procedure for alternative double-hull structure arrangements within the scope of the EU-funded project Crash Coaster, being suggested for adoption in the context of explanatory notes as contained in IMO Resolution A.684(17) (IMO, 1991). The basic concept of this procedure is to compare the critical deformation energies between an original double-hull design and an alternative arrangement in case of side collisions. If the deformation energy of a new arrangement is equivalent or greater than that of the reference structure, it was considered as satisfactory for the safety level defined in SOLAS. Finite Element Analysis (FEA), such as LS-DYNA, PAM-CRASH and ABAQUS, was suggested to carry out the calculation of critical deformation energy. Unfortunately, this approval procedure has not been successfully adopted as IMO Resolution. Instead, the FE analysis method of this procedure was adopted in the "European Agreement concerning the International Carriage of Dangerous Goods by Inland Waterways" in 2008 (UN, 2008) as alternative constructions for double hull structure arrangements of tankers, which is simply known as ADN 2009. In the approval procedure in ADN 2009, the concept of risk (i.e., $Risk = P \times C$, P is

[1] Maritime Safety Research Centre, University of Strathclyde, Glasgow, Scotland, UK
[2] Lead Author

probability of cargo tank rupture and C is consequence of cargo tank rupture by damage measurement) is adopted to compare the risk of a crashworthy construction to that of a reference double-hull design. The probability P is calculated from a predefined function of energy absorption capacity (E) for various collision conditions such as three different collision draughts, three different locations, four different speeds with the maximum of 10m/s, two angles of 55° and 90° and two different bow shapes, while the consequence C is defined as the maximum capacity of the largest cargo tank in alternative and reference designs. However, these approaches are only concerned with structural strength itself, overlooking the ensuing consequences such as ship flooding problems and damage stability.

Therefore, the focus of this paper is placed on the direct assessment to enhance the overall ship survivability, especially p-factors, with the application of crashworthy structure designs as risk control options (RCOs) based on the FE analysis methodology developments. In Section 2, the methodology of quantitative risk assessment with nine steps is suggested, which provides equivalent damage stability criteria to the current SOLAS regulations within the IMO framework in a cost-effective way. The practical demonstration using a reference cruise vessel is described as a case study in Section 3, including vulnerable zone identification, RCOs applications, FE analysis and cost-benefit analysis. A total of 26 RCOs as passive measures have been investigated, and three RCOs have been finally selected as optimum measures.

2 METHODOLOGY

This proposed methodology focuses on vulnerable areas where improved crashworthiness (i.e. reduction of the p-factor) will lead to enhanced survivability using the crashworthy structural design alternatives independent of loss modality (i.e. covering only the vulnerable area extent). Structural crashworthiness analysis using the FE method leads to reduced damage breach distributions at the area of application and the impact on ship survivability under specific flooding scenarios, as illustrated in Figure 1. Risk reduction (i.e. improved survivability) and cost of this Risk Control Option will support a cost-effectiveness analysis using the Gross Cost of Averting a Fatality (GCAF) for ship survivability enhancement. Approval through the AD&A process is required. Improvement in survivability is significant depending on the protected area, and this is further enhanced by filling side void compartments with high expansion foam to reduce asymmetry and to further enhance crashworthiness.

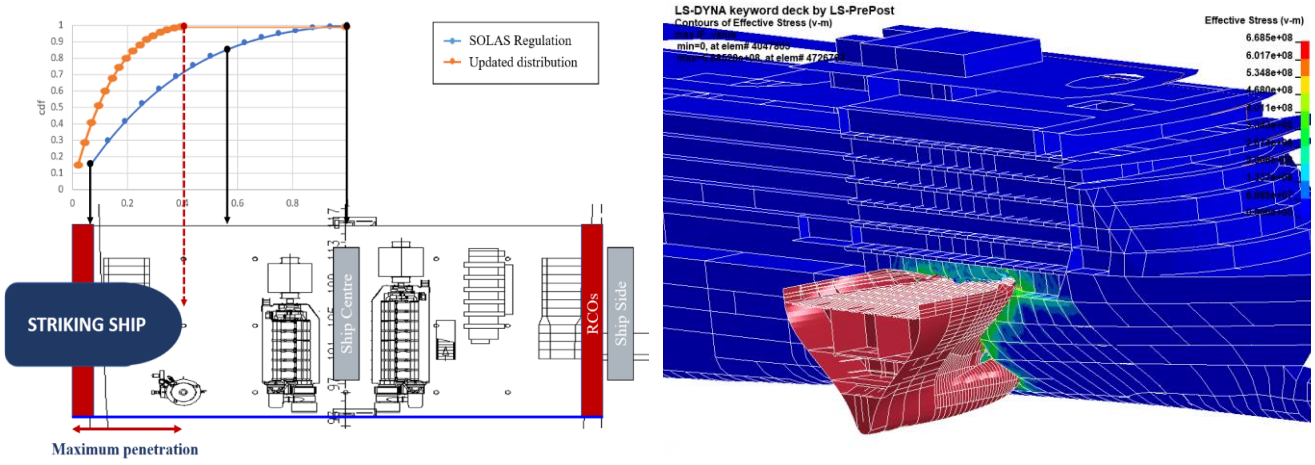

Figure 1: The concept of transverse breach distribution update (Left) based on crashworthiness results (Right)

As a quantitative risk assessment, the proposed methodology consists of nine steps based on the procedure of FEA (IMO, 2018), whilst including the more specific items for collision events, as shown in Table 1.

Table 1: Proposed Methodology compared to IMO FSA Procedure

IMO FSA	Proposed Methodology
STEP 1:Identification of hazard	**STEP 1**: Consideration of current hazard (collision and grounding) **STEP 2**: Vulnerable Zone identification
STEP 2: Risk control options	**STEP 3**: Alternative ship structural design (RCOs)

STEP 3: Risk analysis	**STEP 4**: Collision Scenario Definition **STEP 5**: Structural Crashworthiness Analysis **STEP 6**: Transverse damage breach distribution update **STEP 7**: Damage Stability re-evaluation
STEP 4: Cost-benefit assessment	**STEP 8**: Cost-benefit assessment
STEP 5: Recommendation for decision making	**STEP 9**: Recommendation for decision making

Step 1: Initial Damage Stability Assessment based on SOLAS 2020
First of all, the damage stability of a target ship is calculated through the standard damage stability analysis according to current SOLAS regulations. As a result of the calculation, the p-factor and s-factor of each damage case are obtained along with the current Required Subdivision Index and Attained Subdivision Index.

Step 2: Vulnerable Zone Identification
The next step is to calculate the local Attained Index loss from Equation [1] for the classification of high-risk zones, which enables the identification of the most vulnerable zone in the target ship.

$$Index\ Loss = \sum p_i \times (1 - s_i) \quad [1]$$

Then, one or two high-risk zones can be aimed for RCOs application for ship overall risk improvement. To achieve this, the permeability of each subdivision zone can be manually changed to zero (i.e. no flooding condition) to find how much Index can be improved. However, additional efforts and increased calculation time cannot be avoided for these manual calculations for all relevant compartments. Thus, this paper also proposes a vulnerability analysis method to address these problems.

Step 3: Alternative Design Arrangements as RCOs
The third step of the procedure is to design and apply alternative design arrangements, namely RCOs, to the target zones identified in step 2. In this paper, not only crashworthy arrangement but also additional RCOs, aiming to reduce permeability in the void space created, for example, when using double plates to enhance crashworthiness, also reducing asymmetry during flooding.

Step 4: Collision Scenario Definition
The selection of collision scenarios is a critical factor of the crashworthiness analysis for ship collisions, which directly affects the results of damage breach size. Usually, six aspects are taken into account for collision scenarios: striking ship, collision location, collision speed, collision angle, draught, and trim. Therefore, a reasonable worst scenario has been suggested in this paper within the current SOLAS framework. However, the final collision scenario should be discussed and approved by the relevant Administration based on the target ship's operating areas and profiles.

Striking ship: Firstly, the striking ship mainly relates to the initial kinetic energy with its mass and speed. Additionally, a bow shape directly affects the damage breach results. Therefore, it is reasonable that the actual target striking vessel should be selected instead of applications of generalised bow shapes and assumptions. In this respect, this paper recommends a ship with a high probability of encountering a target ship based on its actual operational profile history, such as the IAS data of the target vessel.

Collision Speed: Next, collision speeds of the striking vessel primarily dominate initial collision kinetic energy, directly influencing breech penetration results. Many authors adopted various collision speeds for their collision analysis, such as 2~10 knots for 179m Ropax (Schreuder et al., 2011), 1.6 ~ 6.0 knots for VLCC (Paik et al., 2017), 0.5 ~ 9.0 knots for 9,000 TEU container ship (Kim et al., 2021), 14 knots for Aframax (Zheng et al., 2007) and even 19.44 knots (10m/s) for 310 LNG carrier (Ehlers et al., 2008). However, it should be noted that the kinetic energy with 19.44 knots is 15 times larger than that with 5 knots, which leads to totally different simulation results. Thus, instead of fixed collision speeds, this paper proposes a "*relative collision speed*" concept, which is the speed resulting in B/2 penetration within the current SOLAS framework, and the collision speed can be identified from pre-simulations of collisions. Two advantages are expected for this approach. The first one is the collision scenario can be decided within the IMO framework (i.e. the maximum penetraion is B/2), which is not too mild or not too severe collision case. The second advantage is that it may minimise or calibrate different damage results caused by simulation set-up uncertainties, such as different failure criteria and material curve effects. Therefore, a series of pre-simulations with various collision speeds must be carried out to find the "relative collision speed" for B/2 penetration, as shown in Figure 2.

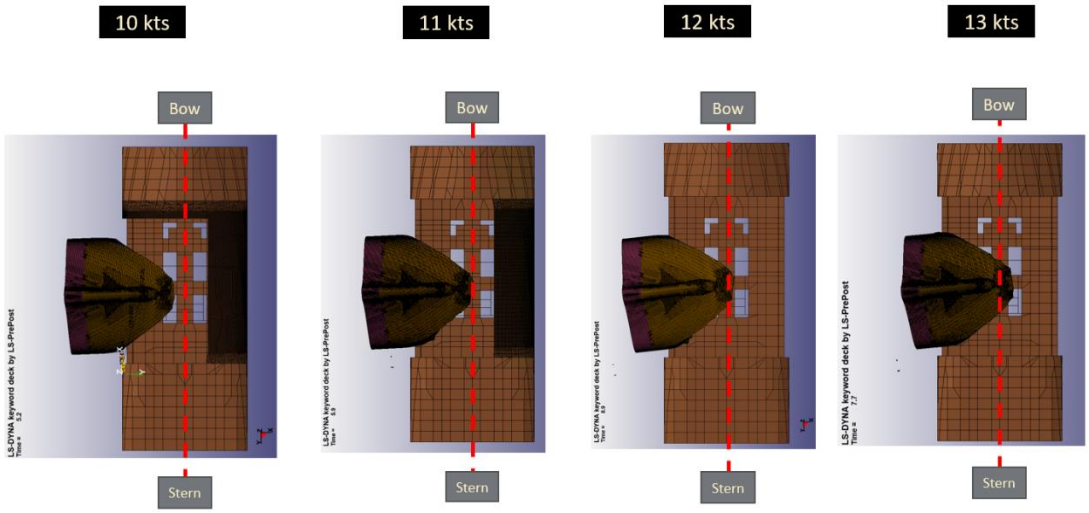

Figure 2 A series of pre-simulated scenarios to find the corresponding collision speed

Collision Location: The collision location is defined as a centre of a vulnerable zone selected in STEP 2, where RCOs will be implemented for damage stability improvement.

Collision Angle: It is generally known that the maximum internal energy occurs at a perpendicular collision when a struck ship is in a static condition. Thus, for a conservative approach, a collision angle of 90° is adopted.

Collision Draught and Trim: Due to draught differences, the relative ships' position may lead to various damage extents. However, in this paper, the collisions are assumed to be taken place at an even trim condition at the design draught.

Step 5: Structural Crashworthiness Analysis

The next step is to carry out ship collision simulations for the target vulnerable zone with different RCOs at the collision scenario determined in the previous step 4. Since the structural response in ship collisions is highly nonlinear, entailing crushing, buckling, plasticity and rupture, the nonlinear finite element method (NLFEM) has been adopted in this paper, which is also recommended in ADN 2009 for alternative structure procedures (UN, 2008). In particular, whilst the FE analysis method in ADN 2009 employs restrain in three transitional freedoms, the actual ship motions with surrounding water effects are taken into account in the proposed methodology using MCOL solver such as added mass effects as well as restoring and wave damping forces. It enables not only reflecting actual external dynamics between the two ships but also coupling dynamics with internal collision mechanics.

Step 6: Transverse Breach Distribution Update

As a result of the simulation results from Step 5, different reduced penetrations may be obtained depending on RCO arrangements. With these reduced penetrations, the target zone's cumulative transverse breach distribution function can be proportionally adjusted from a predetermined SOLAS CDF by shifting the point of 1 from a ship centre (B/2) to a maximum penetration position, as shown in Figure 11. Then, the corresponding PDF can be obtained from the updated CDF for the damage stability recalculation.

Step 7: Damage Stability Re-evaluation

With new RCO arrangements and the updated breach distribution, the damage stability can be recalculated, and the improvement of the Subdivision Attained Index from each ROC can be identified.

Step 8: Cost-Benefit Analysis

The next step is to perform a cost-benefit analysis for an optimum solution among RCOs. As recommended in FSA guideline by IMO (2018), the Gross Cost of Avering a Fatality (GCAF) is used for the cost-effectiveness of each RCO as follows:

$$GCAF = \frac{\Delta Cost}{\Delta Risk} \quad [2]$$

The cost of each RCO includes capital expenditure, such as material and labour cost, and operational cost, such as increased fuel cost due to increased weight from each RCO implementation. For risk reduction, the expected reduction of fatalities (i.e., PLL) is used as a risk reduction factor. For the calculations, the risk models defined in the EMSAIII (2013-2016) project have been employed.

Step 9: Decision-Making and Approval Process of Alternative Design and Arrangement (AD&A)
In the final step, the selected optimum RCOs should be discussed and investigated further for a final decision by the associated decision-makers such as shipowners, shipbuilders, designers, class societies and the Administrations. Then, an approval process may proceed for implementation to the actual construction or modification of the target ship.

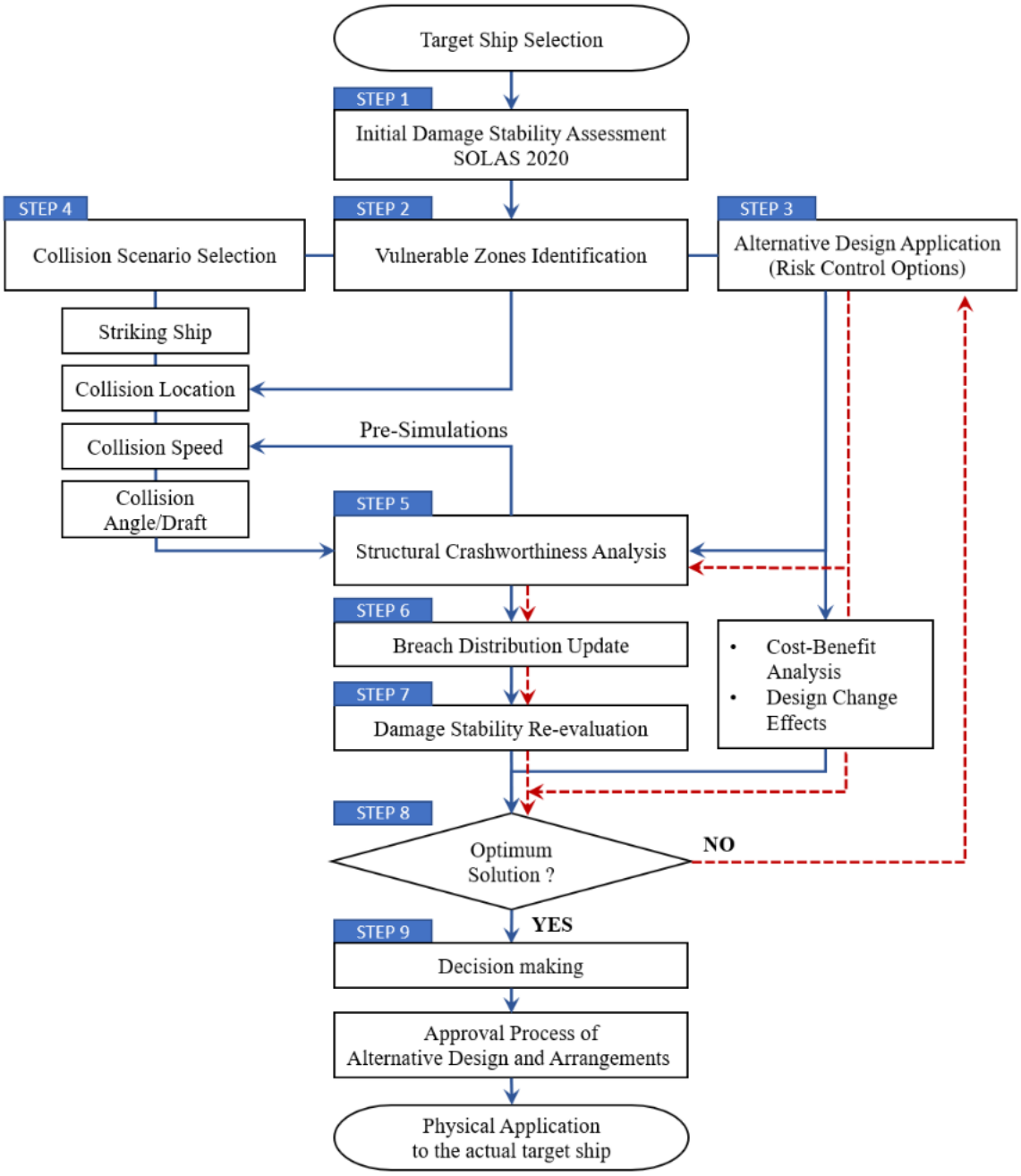

Figure 3: Overall workflow of the proposed methodology

3 CASE STUDY

For demonstration purposes of this proposed methodology, a case study has been carried out for a reference cruise ship, FLOODSTAND SHIP B (Luhmann, 2009) in case of collision by a 45,000 GT RoPax as a striking ship, in Figure 4. The main particulars are shown in Table 2.

Table 2: Main Particulars of the reference ship

	Reference ship (Struck ship)	Striking Ship
LOA /LBP (m)	238.0 / 216.8	221.5 / 200.0
B (m)	32.2	30.0
Design draught (m)	7.2	6.9
Displacement (tonne)	35,367	31,250
Number of persons onboard	2,400	-

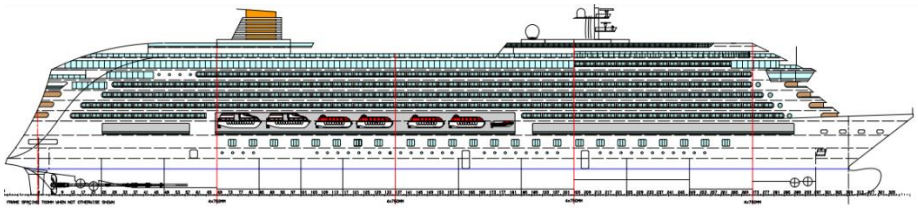

(a)

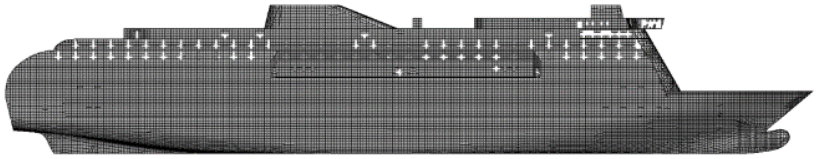

(b)

Figure 4; Employed vessels (a) 63,000GT cruise ship as a reference ship and (b) 45,000GT RoPax as a striking ship

3.1 STEP 1: Initial Damage Stability Assessment

The damage stability evaluation has been performed based on the current SOLAS regulatory framework to identify the risk of the as-built design for the reference vessel. An Attained Subdivision Index of 0.8579 was obtained, which fails to meet the Required Subdivision Index of 0.8676, meaning that it does not fulfil the SOLAS regulations, as summarised in Table 3.

Table 3 : Results of initial damage stability evaluation of the reference ship

Draught (m)		Trim (m)	GM (m)	Partial Indices		Weight coefficient	Attained Index A
Dl	6.890	0.120	2.670	Al	0.87787	0.2	0.1756
Dp	7.196	0.000	2.620	Ap	0.85723	0.4	0.3429
Ds	7.400	0.000	2.720	As	0.84853	0.4	0.3394
Attained Subdivision Index A							**0.8579**
Required Subdivision Index R							0.8676

3.2 STEP 2: Vulnerability Analysis

Based on the damage stability results at STEP1, the local Attained Indies of each zone are presented depending on the number of zone damages compared with the maximum Index, as presented in Figure 5. The latter Index can be calculated when the s-factor is the maximum of 1 (i.e. The maximum local Subdivision Attained Index = $\sum p \times s_{max} = \sum p \times 1$). As indicated in a black dotted rectangle in Figure 5 (c) and (d), the low local Indies of zones between Z11 and Z18 are observed for 3-zone and 4-zone damages cases, which means the ship survivability (s-factor) in case of damages in those zones is relatively low, and therefore they are considered as high-risk zones.

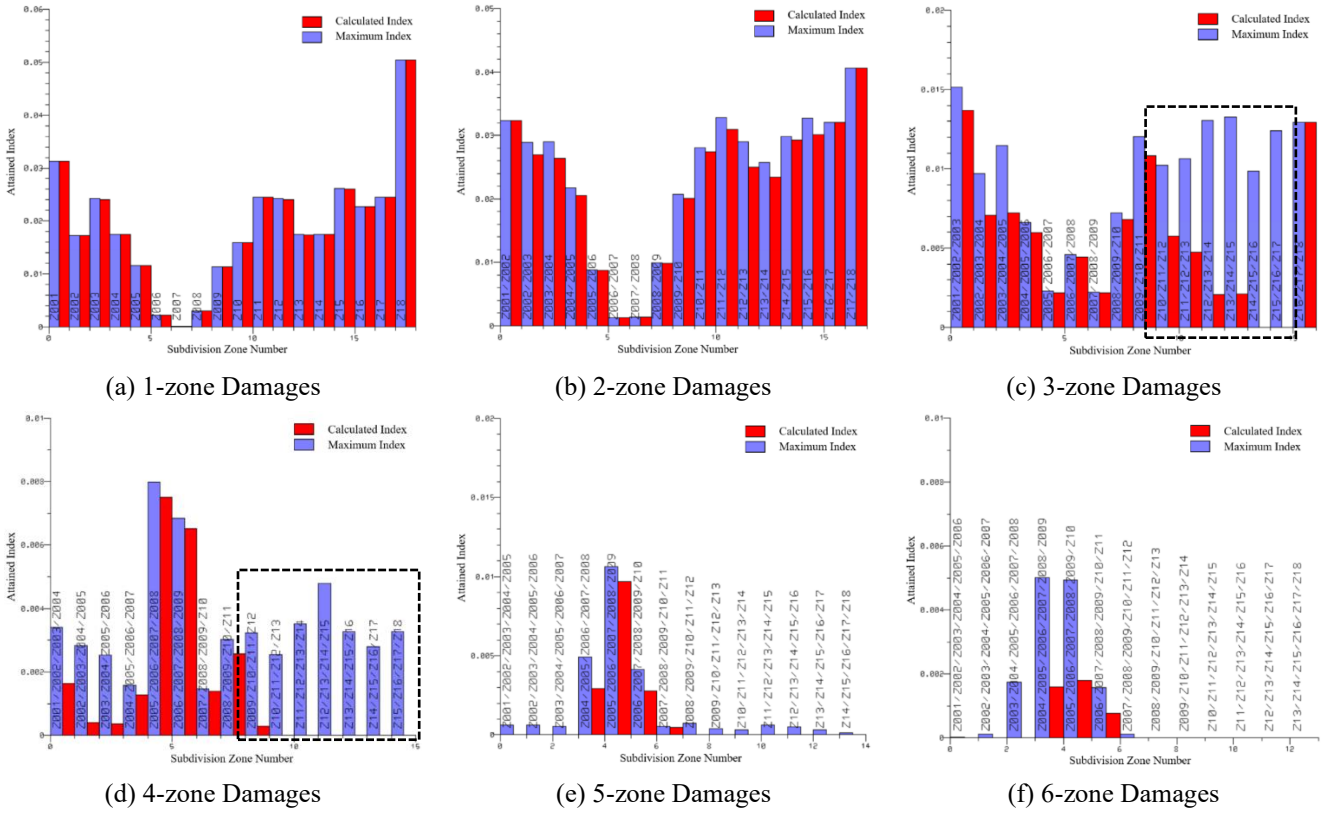

(a) 1-zone Damages (b) 2-zone Damages (c) 3-zone Damages

(d) 4-zone Damages (e) 5-zone Damages (f) 6-zone Damages

Figure 5: Local Attained Indices in red compared with the maximum values in blue

These risks can be quantified using Index loss from Equation [1]. However, the problem is how much Index loss of each zone contributes to the total local Index loss for multi-zone damage cases. In this respect, this paper proposes a plurality approach with extension to adjacent zones as a vulnerability analysis method. This approach assumes that a zone where the damage centre of each multi-damage case locates takes all index loss, which is sometimes called a "winner-take-all" method. Furthermore, the local Attained Indies of the adjacent zones are also improved when the target zone has higher survivability, which means the risks of the adjacent zones are also related to the target zone. Therefore, the risk of the target zone is assumed to be determined from a summation of three-zone risks, such as the target zone itself and two adjacent zones. Bae (2022) has proven this vulnerability analysis compared to individual improvement results of each zone in the maximum survivability condition (i.e. zero permeability). The summary of vulnerability analysis for a reference vessel is shown in Table 4 and Figure 6.

Table 4: Vulnerability analysis results of the reference ship using plurality approach for adjacent zones

	1-zone damage	2-zone damage	3-zone damage	4-zone damage	5-zone damage	6-zone damage	Local Index Loss	Adjacent Zones' Index Loss	Risk ranking
Z1	0.0000	0.0000	0.0000	0.0000	0.0000	0.0000	0.0000	0.0015	18
Z2	0.0000	0.0000	0.0015	0.0000	0.0000	0.0000	0.0015	0.0143	12
Z3	0.0003	0.0045	0.0026	0.0042	0.0012	0.0000	0.0128	0.0244	8
Z4	0.0001	0.0012	0.0042	0.0022	0.0006	0.0019	0.0101	0.0295	7
Z5	0.0000	0.0001	0.0007	0.0003	0.0020	0.0034	0.0065	0.0171	11
Z6	0.0000	0.0000	0.0000	0.0005	0.0000	0.0000	0.0005	0.0081	14
Z7	0.0000	0.0000	0.0001	0.0000	0.0009	0.0000	0.0011	0.0019	17
Z8	0.0000	0.0000	0.0000	0.0003	0.0000	0.0000	0.0003	0.0065	15
Z9	0.0000	0.0001	0.0004	0.0001	0.0014	0.0031	0.0051	0.0087	13
Z10	0.0000	0.0007	0.0012	0.0005	0.0001	0.0008	0.0032	0.0195	9
Z11	0.0000	0.0025	0.0045	0.0029	0.0011	0.0001	0.0112	0.0309	6
Z12	0.0002	0.0040	0.0059	0.0061	0.0003	0.0000	0.0166	0.0417	4
Z13	0.0001	0.0023	0.0110	0.0000	0.0006	0.0000	0.0140	0.0471	3
Z14	0.0000	0.0000	0.0112	0.0048	0.0005	0.0000	**0.0165**	0.0473	2

Z15	0.0001	0.0032	0.0099	0.0033	0.0003	0.0000	0.0168	0.0486	1
Z16	0.0000	0.0000	0.0124	0.0028	0.0001	0.0000	**0.0153**	0.0354	5
Z17	0.0000	0.0000	0.0000	0.0033	0.0000	0.0000	0.0033	0.0186	10
Z18	0.0000	0.0000	0.0000	0.0000	0.0000	0.0000	0.0000	0.0033	16
Total Index Loss							**0.1348**		

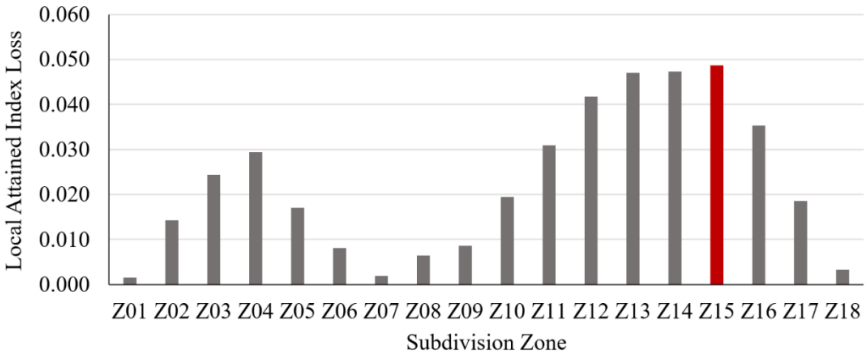

Figure 6: Local Attained Index loss results for a reference ship

3.3 STEP 3: Risk Control Option Applications

Alternative design arrangements as RCOs have been applied to control or mitigate damage stability risks. Table 5 summarises the RCOs taken into account in this case study. A total of 26 RCOs as passive types have been investigated. The passive measures are divided into four specific types: one or two longitudinal bulkheads, strengthened hull thickness, and their combinations. On the other hand, a foam filling measure has been employed as an additional RCO.

Table 5: RCOs adopted in the case study

NO	Name	RCO Type	Description
1	RCO1	Single longitudinal subdivision	Single Longitudinal Bulkhead (LBHD) at B/20
2	RCO2		Single LBHD at 2B/20
3	RCO3		Single LBHD at 3B/20
4	RCO4		Single LBHD at 4B/20
5	RCO5	Double longitudinal subdivision	B/20 LBHD+ Another LBHD (10T) at 13.1m (*)
6	RCO6		2B/20 LBHD+ Another LBHD (10T) at 13.1m (*)
7	RCO7		3B/20 LBHD+ Another LBHD (10T) at 13.1m (*)
8	RCO8		4B/20 LBHD+ Another LBHD (10T) at 13.1m (*)
9	RCO9	Hull thickness change	50% Hull thickness increase
10	RCO10		100% Hull thickness increase
11	RCO11		20T Hull thickness
12	RCO12		30T Hull thickness
13	RCO13		40T Hull thickness
14	RCO14		50T Hull thickness
15	RCO15	Combination of single subdivision and hull thickness change	20T Single LBHD at B/20
16	RCO16		20T Single LBHD at 2B/20
17	RCO17		20T hull + Single LBHD (10T) at 10.6m (*)
18	RCO18		30T hull + Single LBHD (10T) at 6.6m (*)
19	RCO1-F	Structuaral Crashowrthiness RCOs + Foam RCO (Permant Foam Void Filling)	RCO1 + Foam Filling of wing compartments
20	RCO2-F		RCO2 + Foam Filling of wing compartments
21	RCO3-F		RCO3 + Foam Filling of wing compartments
22	RCO4-F		RCO4 + Foam Filling of wing compartments
23	RCO6-F		RCO6 + Foam Filling of wing compartments
24	RCO8-F		RCO8 + Foam Filling of wing compartments
25	RCO17-F		RCO17 + Foam Filling of wing compartments
26	RCO18-F		RCO18 + Foam Filling of wing compartments

3.3.1 Single longitudinal subdivision

This type of passive measure is known as "*double-hull concept*", which is already applied to tankers and LNG carriers to protect the environment from oil spills or gas leakages against ship collisions. The single longitudinal bulkhead on each side is assumed to be installed from a double bottom on deck 1 to embarkation deck on deck 5, as shown in Figure 7 (a). and to be of mild steel with 10mm thickness with no stiffeners. Two wing compartments on both sides formed by each longitudinal subdivision are considered to be connected to each other by cross-flooding devices. In particular, RCOs with four different plate installation positions, such as B/20, 2B/20, 3B/20 and 4B/20, have been examined to study the position effects of each RCO. B/20 is the criteria for double bottom height, whilst B/10 is the position criteria not only for the maximum penetration defined in the current SOLAS Reg.II-1/B-1/8 but also for one of the suggestions for the maximum transverse penetration at the time of SRtP regulation establishment. B/5 is related to the criteria of the maximum damage penetration for RoPax according to the Stockholm Agreement (EU, 2003). For reference, the requirements for tankers with over 5,000m3 fuel oil capacity are between 1.0m and 2.0m depending on fuel oil capacity, according to MARPOL (IMO, 2004).

3.3.2 Double longitudinal subdivision

RCOs with double longitudinal subdivisions aim to form internal safe spaces by installing an additional subdivision just after the maximum penetration point in addition to double-hull arrangements, as shown in Figure 7 (b). The first subdivision, closer to the outer hull, will reduce the penetration absorbing collision energies, whilst the second subdivision makes internal spaces and protects them from flooding following collision. The inner spaces formed by the second subdivision are considered as damage-free spaces called "*safe internal spaces*" and contribute to overall ship survivability (s-factor) improvement by providing additional buoyancy (i.e., reducing amount of floodwater).
Four different positions for the first subdivision are also considered, while the second subdivision position is fixed based on the maximum penetration result.

3.3.3 Hull thickness changes

The third RCO type is to strengthen the hull plate by increasing plate thickness as a simple crashworthy structure arrangement, as illustrated in Figure 7 (c). The advantage of this type of RCO is not to affect the original layout, but it may require a relatively high weight increase and cost conditional on hull thickness. Additionally, a thick enough hull, which does not allow any penetration, can protect the ship from collisions, and the related zone can be considered as an "*unflooded area*". Therefore, a huge improvement in ship survivability can be achieved. On the other hand, if even small openings occur on the strengthened hull, the survivability improvement may be very limited to almost the same as the original layout, even though RCOs are applied. Regarding thickness level, six cases have been considered: Firstly, proportional increases by 50% or 100% for all hull structures have been adopted. Secondly, four identical hull thicknesses of 20T, 30T, 40T and 50T have been taken into account to make RCOs simple.

3.3.4 Passive combination: Single Subdivision + Hull thickness

These RCOs are to combine the previous passive RCO types to create synergy effects using the advantage of each RCO type. For double subdivision RCO type, the second subdivision forms and protect the internal safe spaces keeping buoyancy on the target zone, while the thickened hull may reduce maximum penetration. Therefore, in the combination type of ROC, the strengthened hull will play a role in absorbing more collision energy resisting striking bow penetrations, with a single longitudinal subdivision installed just after the penetration (See in Figure 7 (d)), which is the same as the second subdivision in Section 3.3.2. Two wing compartments are also assumed to be connected to each other. The internal safe spaces and these wing compartments may directly improve ship survivability (s-factor).

3.3.5 Passive combinations with permanent Foam Filling

As shown in Figure 7 (e), the final RCO type is to apply a foam filling system as an additional measure to structural modifications described in the previous section. The concept of this measure is to fill the two wing compartments with high expansion foam permanently, protecting the spaces from being flooded and keeping buoyancy intact in the target zone whilst helping avoid asymmetric floodings. The system was devised by Vassalos and Paterson, and the University of Strathclyde has the patent (Patent No.PCT/ GB2017/050681). The permeability of two wing compartments filled with foam is assumed as 0.05, which was proposed by Paterson (2020). Considering zero permeability for internal safe spaces, the total permeability of the target zone may be between 0.00 and 0.05, which means almost no flooding will occur in the target zone as a "*Never flooded zone*" for this RCO.

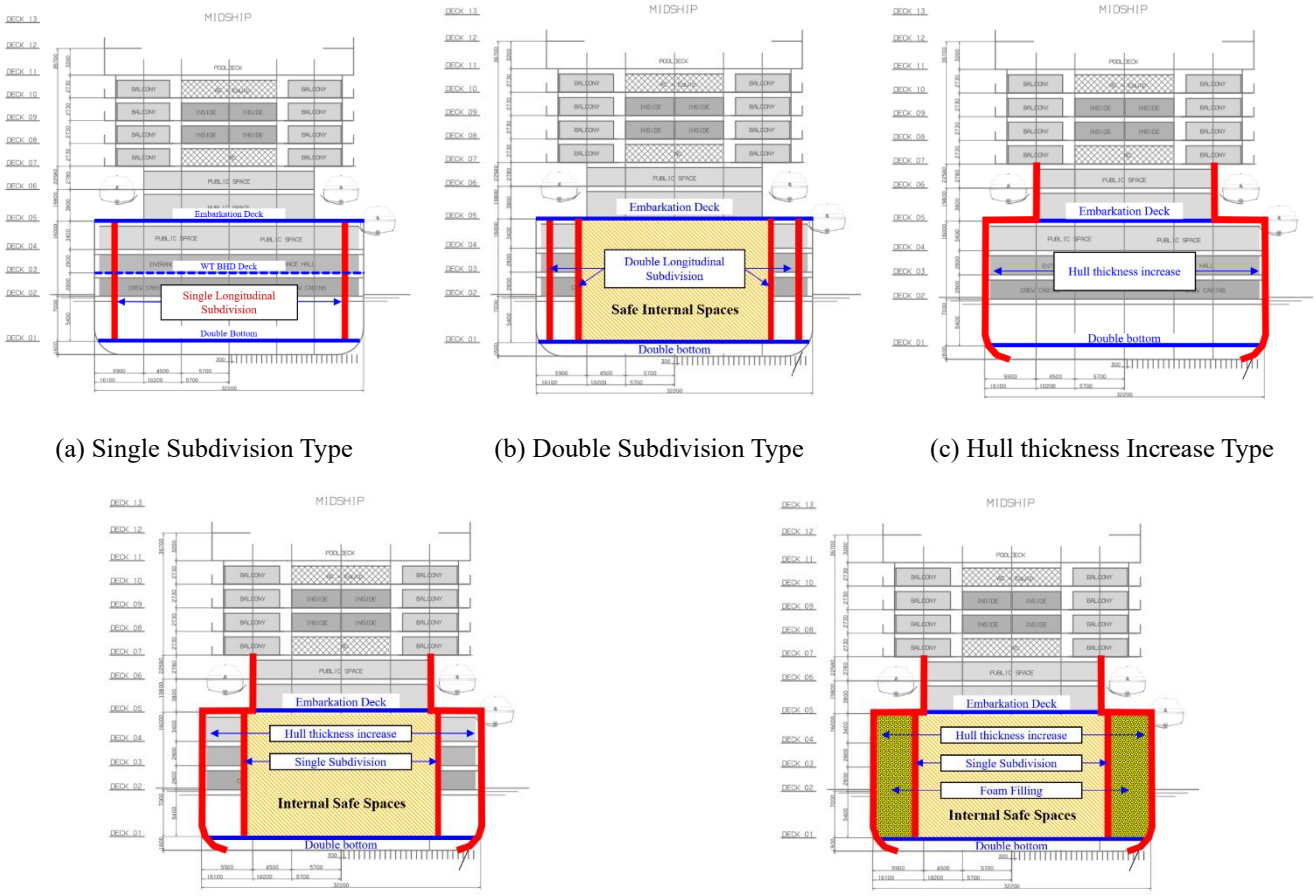

(a) Single Subdivision Type (b) Double Subdivision Type (c) Hull thickness Increase Type

(d) Passive Combination Type (e) Passive Combinations with permanent foam filling

Figure 7: Five different RCOs adopted in the case study

3.4 STEP 4: Collision Scenario Definition

This step is to define a collision scenario, which will be used for finite element analysis in STEP 5. As described in Section 2, six parameters have mainly been considered, such as striking ship, collision speed, collision location, collision angle, draft and trim. The 45,000 GT RoPax has already been designated as the striking ship. Therefore, the striking bow shape and the ship mass have been known from the striking ship drawings and its main particulars, respectively. Zone 15 has been identified as the most vulnerable region of the reference vessel in STEP 2. The collision angle and trim are assumed as 90° and the design draft, respectively. Therefore, the only parameter left is the collision speed.

As defined in the proposed methodology in Section 2, the relative speed generating the maximum penetration of B/2 will be selected as the collision speed in this case study. Therefore, a series of pre-simulations have been carried out to find the speed with B/2 penetration. It should be noted that the same simulation setup for the main FEAs must be used for pre-simulations. Figure 8 illustrates the maximum penetration over time depending on various speeds. The collision speed of 10.14 knots shows the closest transverse penetration to B/2. Therefore, the collision scenario for collision simulations between the reference ship and the striking ship can be summarised in Table 6.

Table 6: Summary of collision scenario for the case study

Ships	speed (knots)	angle (˚)	From A.P. (m)	Draft (m)	Trim (m)
Struck ship	0	0	0	7.2	0
Striking ship	10.14	90	165.8(*)	6.9	0

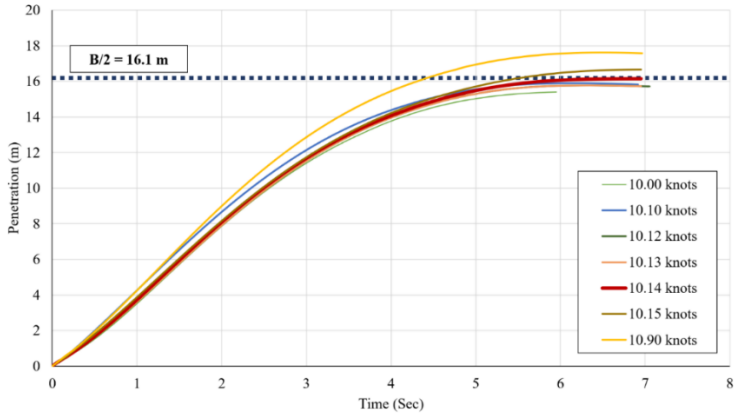

Figure 8: Pre-simulation results for relative collision speed finding

3.5 STEP 5: Structural Crashworthiness Analysis

Next, the collision simulations with each RCO have been carried out using ANSYS/LS-DYNA explicit code for internal mechanics and MCOL solver for external dynamics. The detailed parameters, such as geometric modelling, material property definition, failure criteria, contact and friction, and hydrodynamic boundary definition, are described as follows.

3.5.1 Geometry Modelling

The entire geometry of the reference ship was modelled from zone 1 to zone 18. Fine meshes as deformable regions were applied to the target zone 15 and its adjacent zones, such as Zone 14 and 16, while the rest of the parts were made with coarse meshes and defined as rigid parts. For the striking ship, the forepart of 30.0 m was only considered as the striking ship since it is the only deformation area involved in collisions, and the COG and mass of the striking ship have already been taken into account at MCOL solver (see Section 3.5.5). The forward part of 27.6m was modelled with fine meshes and defined as a deformable part, while the aft part was set to rigid.
The element sizes of the fine meshes for the struck ship and the striking ship are 175mm and 200 mm, respectively, which is a quarter of the frame spacing of each ship and therefore may reasonably capture the structural behaviour economically. It also satisfies the recommendation of fine mesh size (i.e., less than 200mm) defined in AND 2009.
Belytschko-tsay 2D shell elements (LSTC, 2019) with a 5/6 shear factor and 5 through shell thickness integration points have been applied to all geometries, in particular not only for plates but also for stiffeners.

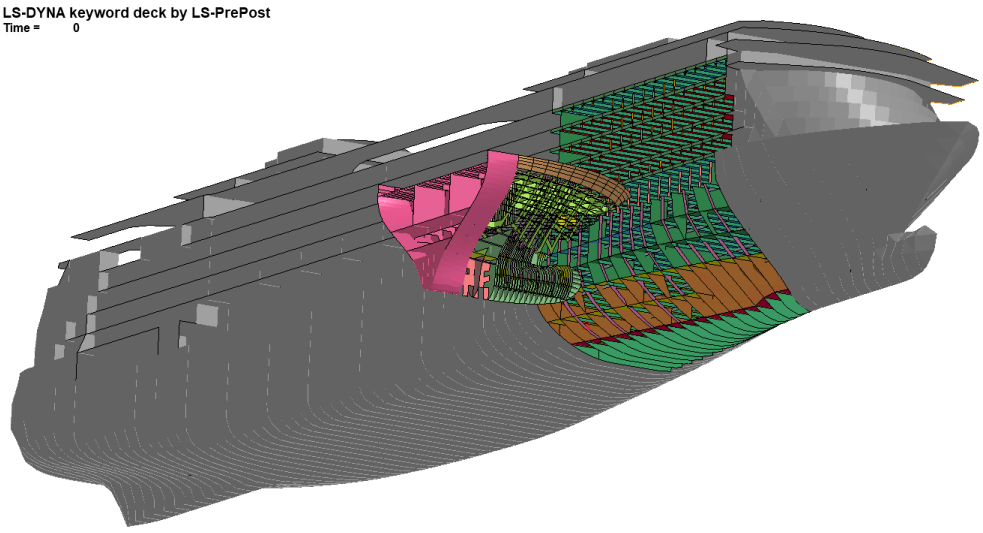

Figure 9: Geometric modellings with 2D shells

3.5.2 Material Property

Both vessels are assumed to be constructed of only mild steel with material properties in Table 7. A material model of Piecewise Linear Isotropic Plasticity (Hodge et al., 1956, LSTC, 2019) has been adopted on the contact regions made of fine meshes for both ships to observe the elastoplastic deformation from collisions. Based on the given material property, a true stress true strain curve in Figure 10 has been applied, which has been modified from the experimental curve (Paik, 2018).

Table 7: Material Properties of mild steel

Parameters	values
Density, ρ (kg/m3)	7850
Young's modulus, E (MPa)	205,800
Poisson's ratio	0.3
Yield stress, σY (Mpa)	235
Ultimate tensile strength (Mpa)	400

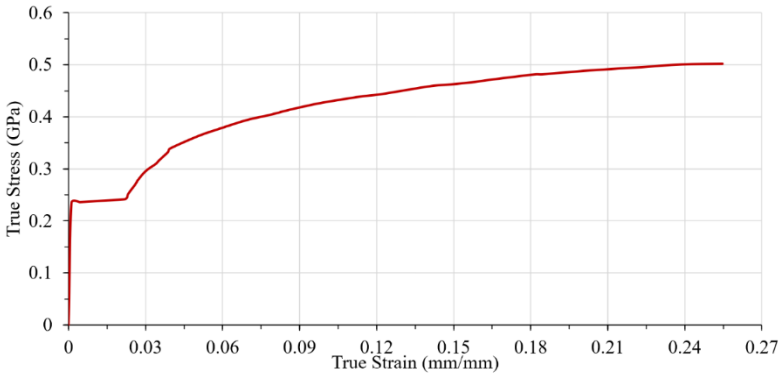

Figure 10: True stress-true strain curve

3.5.3 Failure Criteria and Dynamic Effects

The structural response under impact loading is based on the given stress-strain curve defined in the previous section. However, the most important aspect is to estimate the fracture point of the structures in finite element analysis. Many authors have studied and suggested various failure criteria such as conventional constant failure strain, element size-dependent criteria based on Barba's law (Barba, 1880), forming limit diagram based on strain-based failure criteria, stress state-based failure criteria such as stress triaxiality and failure criteria with consideration of crack propagation. However, it is hard to select the best failure criteria as the FEA results vary depending on the material properties, geometries and collision scenarios. Therefore, in this paper, the through-thickness strain criterion proposed by Vredeveldt (2001) in Equation [3], which is well-known as "GL criterion" and element size-dependent, has been adopted for the collision simulations in this case study. It is simple and the most common failure criterion for FE analysis (IMO, 2003, UN, 2008).

$$\varepsilon_c = \varepsilon_g + \varepsilon_e \frac{t}{l_e} \quad [3]$$

where, ε_c denotes critical fracture strain represented as $\varepsilon_{3f} = \varepsilon_c / (1 + \varepsilon_c)$, thinning strain ε_{3f} may be obtained from $\varepsilon_{3f} = -0.5(\varepsilon_1 + \varepsilon_2)$ based on the incompressibility condition with the Poisson ratio of 0.5. Uniform strain ε_g and necking strain ε_e were defined in Table 8 for different element types used in simulations.

Table 8: Uniform and necking strain values for different element types (Scharrer et al., 2002)

Strain	1-Dimension Structure	2-Dimension Structure
ε_g	0.079	0.056
ε_e	0.760	0.540
Element Type	Beam, Truss	Shell, Plate

Furthermore, it is well known that high strain rates affect the strain-stress curves increasing dynamic yield stress, and the strain rates are influenced by the initial collision energies depending on collision speed changes. Therefore, strain rate effects should be considered for the collision simulations with a relatively high speed. In this respect, Cowper and Symonds formulation (Cowper and Symonds, 1957) has been applied to reflect strain rates effects as follows:

$$\frac{\sigma_{Yd}}{\sigma_Y} = 1.0 + \left(\frac{\dot{\varepsilon}}{C}\right)^{1/q} \quad [4]$$

Where σ_{Yd} and σ_Y are dynamic and static yield stresses, $\dot{\varepsilon}$ is strain rate, C and q are coefficients determined on the basis of test data. For mild steel, C=40.4 and q=5 have been used.

Table 9 summarises the failure strains applied to FE analysis in this case study, which vary depending on the plate thicknesses for both ships.

Table 9: Calculated failure strains for struck and striking ships

Struck ship		Striking ship	
thickness (mm)	Fracture strain	thickness (mm)	Fracture strain
5	0.0671	8	0.0723
6	0.0693	10	0.0763
7	0.0715	11.5	0.0794
8	0.0737	12	0.0804
10	0.0782	13.5	0.0834
12	0.0826	15	0.0865
13	0.0848	19.5	0.0956
14	0.0871	20	0.0966
15	0.0893	25	0.1068
20	0.1004	30	0.1169

3.5.4 Contact and Friction Definition

The node-on-segment penalty method was adopted for contact definition. For this purpose, the "Automatic Single Surface" option in LS-DYNA for contact was used for the FE analysis setup. Regarding the friction between two colliding bodies, it is true that the friction coefficient affects the simulation results, as the initial collision energy should be separately imposed on both friction and internal energy. If friction energy becomes large, the internal energy will be small. Vice versa is the same. Therefore, the friction coefficient should also be carefully selected. According to the engineering handbook, 0.09 ~ 0.19 for lubricated mild steel surfaces and a coefficient of 0.57 for non-lubricated are recommended. On the other hand, industry practice and many works of literature, including Sajdak and Brown (2005) and Paik (2007), recommend dynamic friction coefficients of 0.1~ 0.3 to simplify problems. Under consideration of the hull conditions of normal vessels, which are generally polluted by biofoulings, a value of 0.3 for the dynamic friction coefficient seems to be reasonable.

3.5.5 Hydrodynamic boundary Definition

Many collision simulations in the past generally restrained translational degrees of freedom. However, the actual hydrodynamic boundary conditions for ship collisions are critical as the external dynamics of both ships are involved, such as restoring forces associated with ship mass and buoyancy, added mass of both ships and wave damping forces. In this paper, MCOL solver embedded in LS-DYNA was employed to take into account those ship motions and added mass for FE analysis. The input parameters were calculated from ANSYS AQWA (ANSYS, 2019) based on the ship characteristics in Table 10.

Table 10: Ship characteristics for ship hydrodynamic motions

Parameters		Struck ship	Striking ship
Draft (m)		7.2	6.9
Displacement (tonne)		35,367	31,250
LCG (m)		99.29	85
KG (m)		15	14
Gyration radius (m)	x-direction (Surge)	10.95	11
	y-direction (Sway)	54.20	55
	z-direction (Heave)	56.37	55

3.5.6 FE analysis results

Based on the above simulation setup and collision scenario in STEP 4, a series of simulations have been carried out for each RCO with a 10.14 m/s collision speed. Table A1 in Appendix A shows the summary of the penetration results computed from FEA for each RCO.

3.6 STEP 6: Transverse Breach Distribution Update

Based on the FA analysis results, especially for penetrations, the local transverse distribution of zone 15 can be updated. Figure 11 shows the updated PDF and CDF of RCO18-F compared to the original distribution defined in the current SOLAS regulation for p-factor. The new CDF was adjusted proportionally by penetration reduction, shifting the maximum penetration point from 16.1m (B/2) to the calculated value of 6.58m, which is measured from the hull of the struck ship. Accordingly, the new PDF also can be derived from the new CDF. Then, the new PDF (i.e. new p-factor) as indicated with a blue dotted rectangle can replace the original PDF (i.e. old p-factor). Then, the p-factor of damage cases between 0 and 6.58 will be increased, multiplying by s-factors and leading to local Attained Index improvements. If there are increases in s-factor by RCO arrangement, a bigger Attained Index improvement can be achieved.

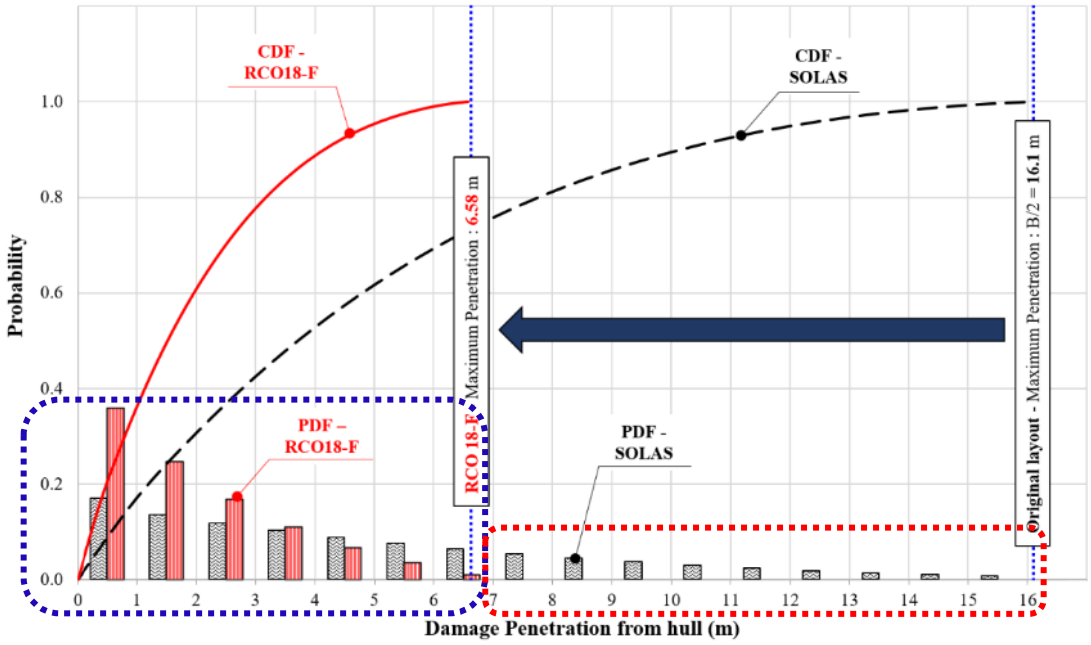

Figure 11: Transverse breach distribution update for RCO18-F

3.7 STEP 7: Damage Stability Re-evaluation

With the implemented RCO arrangement and local transverse breach distribution (p-factor) on the target zone 15, the damage stability of the reference ship has been reassessed, based on the current SOLAS regulations, to identify the overall improvement in the Attained Index. Figure 12 illustrates the damage stability results of RCO18-F, showing differences from the original calculations for the p-factor, s-factor and local Attained Index.

Since the breach distribution of Zone 15 has been updated, the local p-factor of the zone has been changed. Whilst the damage cases in a blue dotted rectangle in Figure 12 (a) have increased p-factors due to PDF increase as indicated in a blue dotted rectangle in Figure 11, those in a red dotted rectangle show p-factor decrease due to excluding the original p-factors between 6.58 and 16.1 as indicated in a red dotted rectangle in Figure 11.
On the other hand, Figure 12 (b) indicates that local s-factors have been improved by applying the RCO arrangement to zone 15. Interestingly, the RCO influence not only the target zone but also adjacent zones, which provides the relevant risks to adjacent zones for vulnerability analysis in STEP 2.
Therefore, the local Attained Indices (i.e. $\sum p - factor \times s - factor$) show both increase and decrease due to p- and s-factor changes in Figure 12 (c), but the overall Attained Index has been increased by 4.5 % from 0.8579 to 0.9005. The damage stability re-assessment results are summarised in Table A1 in Appendix A.

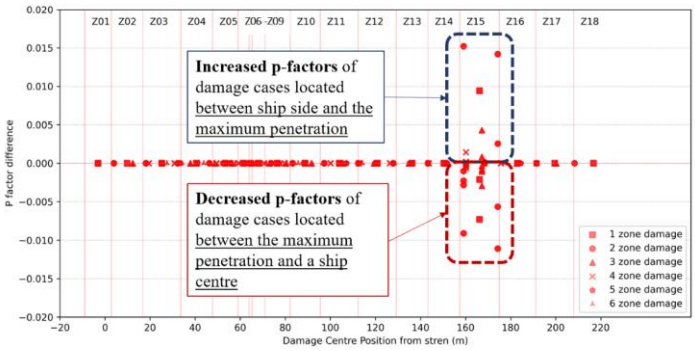

(a) p-factor changes

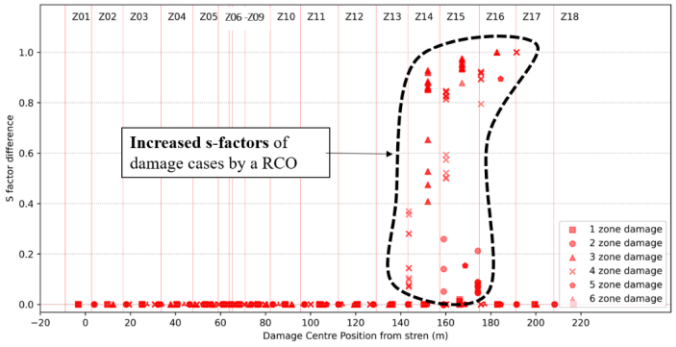

(b) s-factor changes

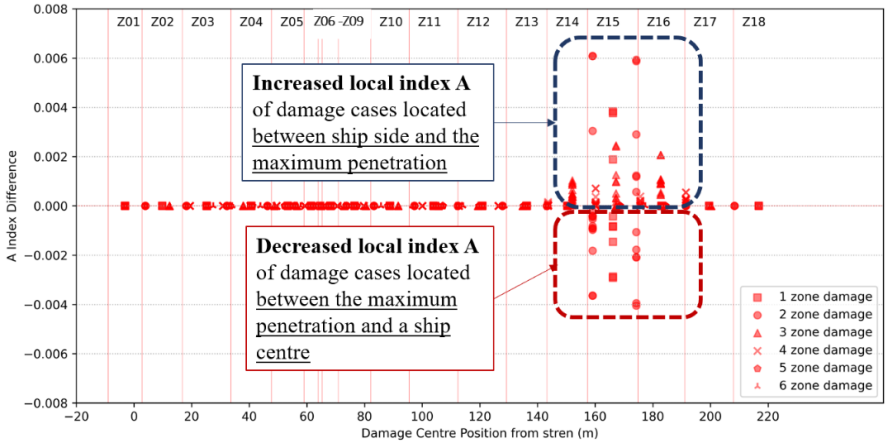

(c) Local Attained Index changes

Figure 12: RCO18-F – Damage stability re-evaluation results

3.8 STEP 8: Cost-Benefit Analysis

The final step is the selection of an optimum solution(s) among RCOs using cost-benefit analysis with GCAF (i.e. $GCAF = \Delta Cost \,/\, \Delta Risk$).

For the cost estimation of each RCO, the unit cost utilised in the EMSA III project in Table 11 has been adopted considering an exchange rate of 1.1 between Euro and USD in 2015. In particular, for foam filling, 600 € /m3 and 25 kg/m3 have been considered based on the relevant study by Paterson (2020). For the additional fuel cost due to the increased weights of each RCO, the wetted area increases have been calculated from NAPA, and it was assumed that it directly affects ship fuel consumption as friction resistance of the ship as a function of the wetted surface area generally takes a majority of total ship resistance. 60% of HFO, 20% of MGO and 20% of low sulphur HFO are presumed to cost 600, 900 and 840 USD/ton, respectively (EMSA, 2015).

Table 11: Unit cost employed for the case study

Description	Unit Cost
Steel weight, including piping, ducting, painting	6,600 USD/ton
Public areas, including ducting, cabling etc	3,300 USD/m2
Cabin areas, including ducting, cabling	2,750 USD/ m2
Service areas, like gallery, laundry including ducting, cabling etc	2,750 USD/ m2
Additional Watertight Sliding Door, including cabling (*)	33,000 USD/pcs
Cost for penetration watertight subdivision including ducting and cabling etc.(*)	275 USD/m2
Additional installed power of main engines, taking into account any discrete step in engine size	418 USD/kW

(*)An additional 20% of the door cost is included for penetrations of ducting and cabling on the subdivision.

ΔPLL as the expected reduction of fatalities was used for risk reduction ($\Delta risk$). The same method employed in EMSAIII (2013-2016) was adopted for PLL calculations:

$$PLL_{total} = PLL_{collision} + PLL_{grounding/contact} + PLL_{fire/explosion} \quad [5]$$

The risk models for collisions and groundings defined in the EMSA III project (see in Figure B1 and C1 in Appendix B and C) have been employed, but the sinking probability in those modes has been updated by the final Attained Index of each RCO calculated in STEP 7 as indicated in a red dotted rectangle in Figure B1 and C1.

4 RESULTS AND DISCUSSIONS

Table A1 in Appendix A summarises the results of the proposed methodology of all 26 RCOs applied to the reference ship, including the maximum penetration obtained from FEA, the total cost of each RCO, risk reduction based on the final damage stability recalculations and GCAF values as the results of cost-benefit analysis.

In particular, the GCAF results obtained from the cost-benefit analysis are plotted with the corresponding Subdivision Attained Index of each RCO, as shown in Figure 13. According to the graph, the RCO14, which has a hull thickness of 50T, was identified as the most effective measure with a GCAF of 1.32 due to no penetrations on the hull for the given collision scenario, providing the highest survivability of 0.9008 with a relatively high cost of 2.74 million USD. However, since the design of RCO is a single hull concept, it may have potential risks from structural defects of the hull, such as corrosion, then the target zone cannot avoid being flooded. RCO18-F, which has 30T hull and a Single LBHD at 6.6m along with a permanent foam filling system in two wing compartments, shows a GCAF of 1.15 with a similar improvement as RCO14 with the Subdivision Attained Index of 0.9005 and the RCO cost of 2.90 million USD, which is more reliable measure with a double-hull arrangement. Furthermore, a foam filling system may flexibly control risks from collisions. On the other hand, RCO18 as the only passive type may be a good alternative measure, which also shows significant improvement in ship survivability with Attained Subdivision Index of 0.8925 and 1.84 million USD cost resulting in a GCAF of 1.09.

With these three optimum solutions, the associated decision-makers should make the final decision considering the company's financial condition, company operational philosophy, and construction periods.

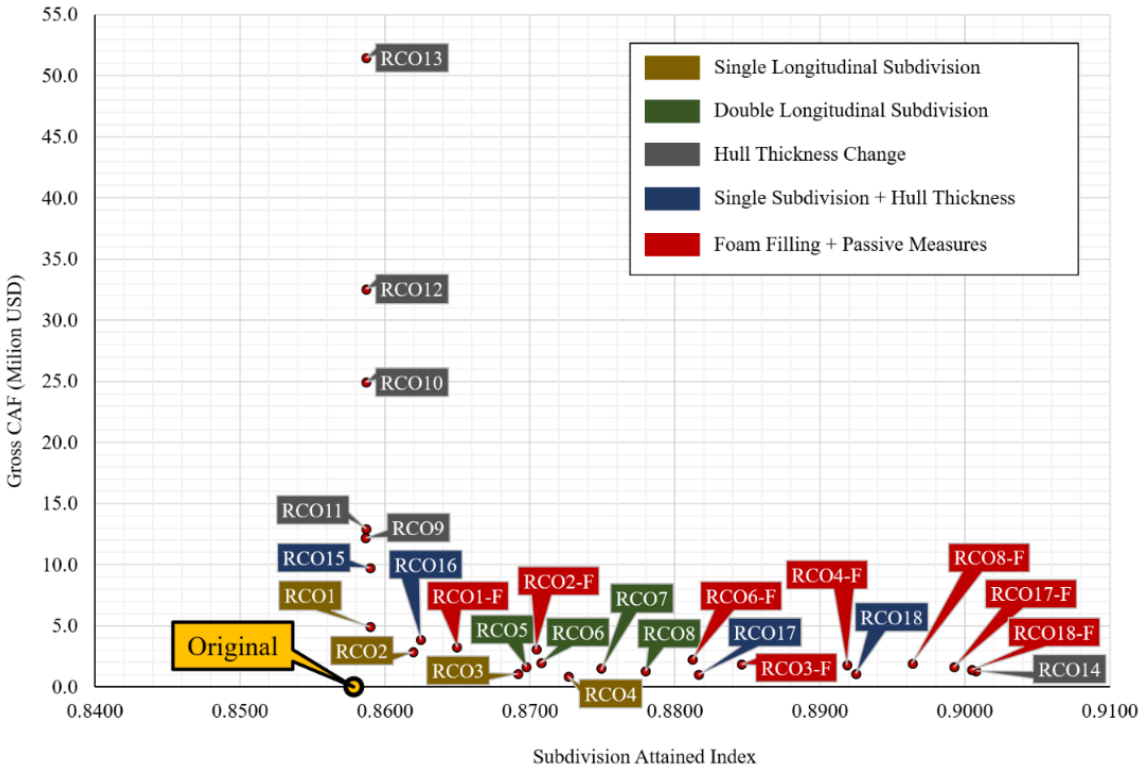

Figure 13: Cost-benefit analysis results for all RCOs

5 CONCLUSION

This paper suggested a methodology of ship survivability improvement based on using crashworthy structures to suitably affect p-factor distributions in targeted ship sections, enabling crashworthy structure assessment, which the current SOLAS framework cannot cover. The proposed methodology with nine steps has been demonstrated for a 65,000 GT cruise ship as a case study. A total of 26 RCOs have been considered for risk control or mitigation purposes. Using vulnerability analysis with the plurality approach with extension to adjacent zones, Zone 15 has been identified as the target zone and collision location. A collision speed of 10.14 knots resulting in the maximum B/2 penetration, has been selected from a series of pre-simulations. Based on the defined collision scenario, collision simulations of each RCO have been carried out using FE analysis and obtained the corresponding penetration reduction results. Then, the local transverse breach distribution of the target zone for each RCO was updated based on the calculated maximum penetrations and reflected in the final damage stability calculation. Then, a cost-benefit analysis has been followed for each RCO. The cost involves both CAPEX and OPEX, such as material, labour and fuel oil costs. The PPL reduction of each RCO has been calculated using the risk models in the EMSAIII project and the results of damage stability re-assessment of each RCO. Finally, three RCOs of RCO14, RCO18 and ROC18-F among all 28 RCOs have been identified as optimum solutions, which are the single-hull type with 50T hull thickness, double hull type with 30T hull and single subdivision at 6.6m, permanent foam filling application to ROC18, respectively. Based on the suggested RCOs, the final decision will be made by the associated decision-makers, and the "approval process of alternative design and arrangement (AD&A)" will be followed for the actual implementation of the final RCO.
In particular, for RCO 18 and RCO18-F as a double-hull concept, more flexible and spacious internal spaces can be achieved if the RCO applies to the adjacent zones and the target zone. Then, it may provide significant design innovations for ships in the future.

6 ACKNOWLEDGEMENTS

The research presented in the paper has been carried out under support from DNVGL and RCCL, sponsors of the MSRC. However, the opinions expressed herein are those of the authors and do not reflect the views of DNVGL and RCCL.

7 REFERENCES

ANSYS 2019. User's manual for ANSYS AQWA version 18. *In:* INC., A. (ed.). PA, USA.

BARBA, M. 1880. Mémoires de la Société des Ingénieurs Civils. *Memoirs of the Society of Civil Engineers,* 22.

COWPER, G. R. & SYMONDS, P. S. 1957. Strain-hardening and strain-rate effects in the impact loading of cantilever beams. Brown Univ Providence Ri.

EHLERS, S., BROEKHUIJSEN, J., ALSOS, H. S., BIEHL, F. & TABRI, K. 2008. Simulating the collision response of ship side structures: a failure criteria benchmark study. *International Shipbuilding Progress,* 55**,** 127-144.

EMSA 2015. Risk Acceptance Criteria and Risk Based Damage Stability, Final Report, Part 2: Formal Safety Assessment.

EMSAIII 2013-2016. Study assessing the acceptable and practicable risk level of passenger ships related to damage stability ("EMSA 3"), undertaken by DNVGL. EMSA/OP/10/2013, http://emsa.europa.eu/damage-stability-study.html.

EU 2003. THE EUROPEAN PARLIAMENT AND OF THE COUNCIL of 14 April 2003 on specific stability requirements for ro-ro passenger ships. *DIRECTIVE 2003/25/EC.* Official Journal of the European Union.

HARDER 2000-2003. Harmonisation of Rules and Design Rationale. EC Contact No. GDRB-CT-1998-00028, Final Technical Report.

HODGE, P., HOPKINS, H. & LEE, E. 1956. The theory of piecewise linear isotropic plasticity. *Deformation and Flow of Solids/Verformung und Fliessen des Festkörpers.* Springer.

IMO 1991. Expanatory notes to the SOLAS regulation on subdivision and damage stability of Cargo ships of 100 meters in length and over. *Res.A.684(17).* the Assembly, International Maritime Organisation, London, UK.

IMO 2003. DEVELOPMENT OF EXPLANATORY NOTES FOR HARMONIZED SOLAS CHAPTER II-1, Approval procedure concept for alternative arrangements, Submitted by Germany. *SLF 46/INF.10.* SUB-COMMITTEE ON STABILITY AND LOAD LINES AND ON FISHING VESSELS SAFETY, International Maritime Organisation, London, UK.

IMO 2004. Amendments to the Annex of the Protocol of 1978 relating to the International Convention for the Prevention of Pollution From Ships, 1973. *Res.MEPC.117(52) Reg.19 & 20.* Marine Environment Protection Committee, International Maritime Organisation, London, UK.

IMO 2018. Revised Guidelines for Formal Safety Assessment (FSA) for use in the IMO Rule Making Process. *In:* 2, M.-M. C. R. (ed.) *Maritime Safety Committee & Marine Environmental Protection Committee, International Maritime Organisation, London, UK.*

KIM, S. J., KORGERSAAR, M., AHMADI, N., TAIMURI, G., KUJALA, P. & HIRDARIS, S. 2021. The influence of fluid structure interaction modelling on the dynamic response of ships subject to collision and grounding. *Marine Structures,* 75**,** 102875.

LSTC 2019. LS-DYNA keyword user's manual. *In:* CORPORATION, L. S. T. (ed.). California, USA.
LUHMANN, H. 2009. Floodstand WP1 Deliverable D: Concept ship desing B.
PAIK, J. 2007. Practical techniques for finite element modeling to simulate structural crashworthiness in ship collisions and grounding (Part I: Theory). *Ships and Offshore Structures,* 2**,** 69-80.
PAIK, J. K. 2018. *Ultimate limit state analysis and design of plated structures*, Wiley Online Library.
PAIK, J. K., KIM, S. J., KO, Y. K. & YOUSSEF, S. A. Collision risk assessment of a VLCC class tanker. SNAME Maritime Convention, 23-28 October 2017 2017 Houston, USA. The Society of Naval Architects and Marine Engineers.
PATERSON, D. 2020. *Reconfiguring the ship environment for damage stability enhancement.* University of Strathclyde.
SAJDAK, J. & BROWN, A. 2005. Modeling longitudinal damage in ship collisions. *SSC-437, Ship Structure Committee*.
SCHARRER, M., ZHANG, L. & EGGE, E. 2002. Kollisionsberechnungen in schiffbaulichen entwurfssystemen (collision calculation in naval design systems). Bericht ESS 2002.183. *Germanischer Lloyd*.
SCHREUDER, M., HOGSTRÖM, P., RINGSBERG, J. W., JOHNSON, E. & JANSON, C. E. 2011. A method for assessment of the survival time of a ship damaged by collision. *Journal of ship research,* 55**,** 86-99.
UN 2008. European Agreement concerning the international Carriage of Dangerous Goods by Inland Waterways (ADN). *ECE/TRANS/203 (Vol.I).* United Nations, New York and Geneva.
VASSALOS, D., MUJEEB-AHMED, M., PATERSON, D., MAURO, F. & CONTI, F. 2022. Probabilistic damage stability for passenger ships—the p-factor illusion and reality. *Journal of Marine Science and Engineering,* 10**,** 348.
VREDEVELDT, A., FEENSTRA E 2001. Crashworthy side structures for improved collision damage survivability of coasters and medium sized Ro-Ro cargo ships.
ZHANG, L., EGGE, E.-D. & BRUHNS, H. 2004. *Approval procedure concept for alternative arrangements*, Germanischer Lloyd.
ZHENG, Y., AKSU, S., VASSALOS, D. & TUZCU, C. 2007. Study on side structure resistance to ship-ship collisions. *Ships and Offshore Structures,* 2**,** 273-293.

APPENDIX

A. Summary of the proposed methodology results for all RCOs

Table A1: Result summary for all RCOs

NO	RCO	Description	Penetration (m)	Attained Index	Weight increase (Ton)	Cost (Mil $)	Δ PPL	GCAF
	Original	**Original Layout**	**16.15**	**0.8579**	-	-	-	-
1	RCO1	Single LBHD at B/20	13.13	0.8590	28.14	0.27	0.05	4.96
2	RCO2	Single LBHD at 2B/20	13.03	0.8619	31.58	0.57	0.20	2.84
3	RCO3	Single LBHD at 3B/20	11.82	0.8692	34.67	0.59	0.55	1.07
4	RCO4	Single LBHD at 4B/20	12.51	0.8727	37.42	0.62	0.72	0.86
5	RCO5	1st LBHD at B/20 + 2nd LBHD (*)	13.13	0.8698	70.36	0.94	0.58	1.62
6	RCO6	1st LBHD at 2B/20 + 2nd LBHD (*)	13.03	0.8708	73.80	1.24	0.63	1.96
7	RCO7	1st LBHD at 3B/20 + 2nd LBHD (*)	11.82	0.8749	76.88	1.27	0.83	1.52
8	RCO8	1st LBHD at 4B/20 + 2nd LBHD (*)	12.51	0.8780	79.63	1.30	0.98	1.32
9	RCO9	50% Hull thickness increase	11.72	0.8587	49.51	0.47	0.04	12.19
10	RCO10	100% Hull thickness increase	8.22	0.8587	99.03	0.97	0.04	24.94
11	RCO11	20T Hull thickness	10.46	0.8587	52.58	0.50	0.04	12.95
12	RCO12	30T Hull thickness	6.58	0.8587	128.38	1.26	0.04	32.55
13	RCO13	40T Hull thickness	6.64	0.8587	204.18	1.99	0.04	51.47
14	**RCO14**	**50T Hull thickness**	**0**	**0.9008**	**279.98**	**2.74**	**2.08**	**1.32**
15	RCO15	20T Single LBHD at B/20	10.14	0.8590	56.29	0.54	0.06	9.75
16	RCO16	20T Single LBHD at 2B/20	10.31	0.8625	63.17	0.87	0.23	3.85
17	RCO17	20T hull + Single LBHD at 10.6m (**)	10.46	0.8816	92.15	1.16	1.16	1.00
18	**RCO18**	**30T hull + Single LBHD at 6.6m (**)**	**6.58**	**0.8925**	**161.55**	**1.84**	**1.69**	**1.09**
19	RCO1-F	RCO1 + Foam System	13.13	0.8650	56.73	1.12	0.35	3.24
20	RCO2-F	RCO2 + Foam System	13.03	0.8704	75.51	1.89	0.61	3.07

21	RCO3-F	RCO3 + Foam System	11.82	0.8846	95.18	2.43	1.31	1.86
22	RCO4-F	RCO4 + Foam System	12.51	0.8919	114.59	2.96	1.66	1.78
23	RCO6-F	RCO6 + Foam System	13.03	0.8812	117.73	2.58	1.14	2.26
24	RCO8-F	RCO8 + Foam System	12.51	0.8964	156.81	3.63	1.88	1.93
25	RCO17-F	RCO17 + Foam System	10.46	0.8993	162.75	3.29	2.03	1.63
26	**RCO18-F**	**RCO18 + Foam System**	**6.58**	**0.9005**	**196.62**	**2.90**	**2.07**	**1.40**

(*) 13.1 m from the outer shell of the hull
(**) Distance from the outer shell

B. Collision risk model

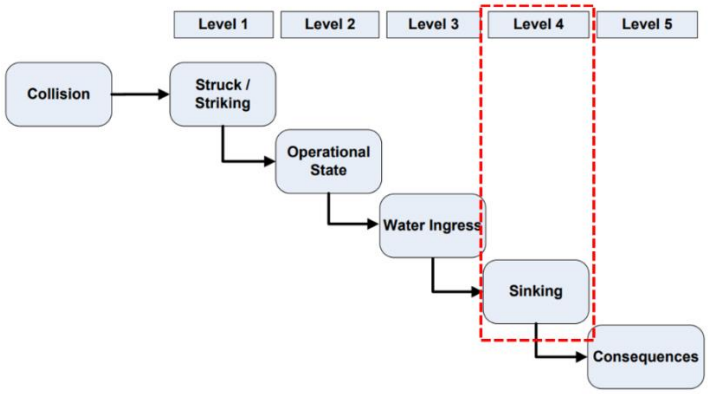

(a)

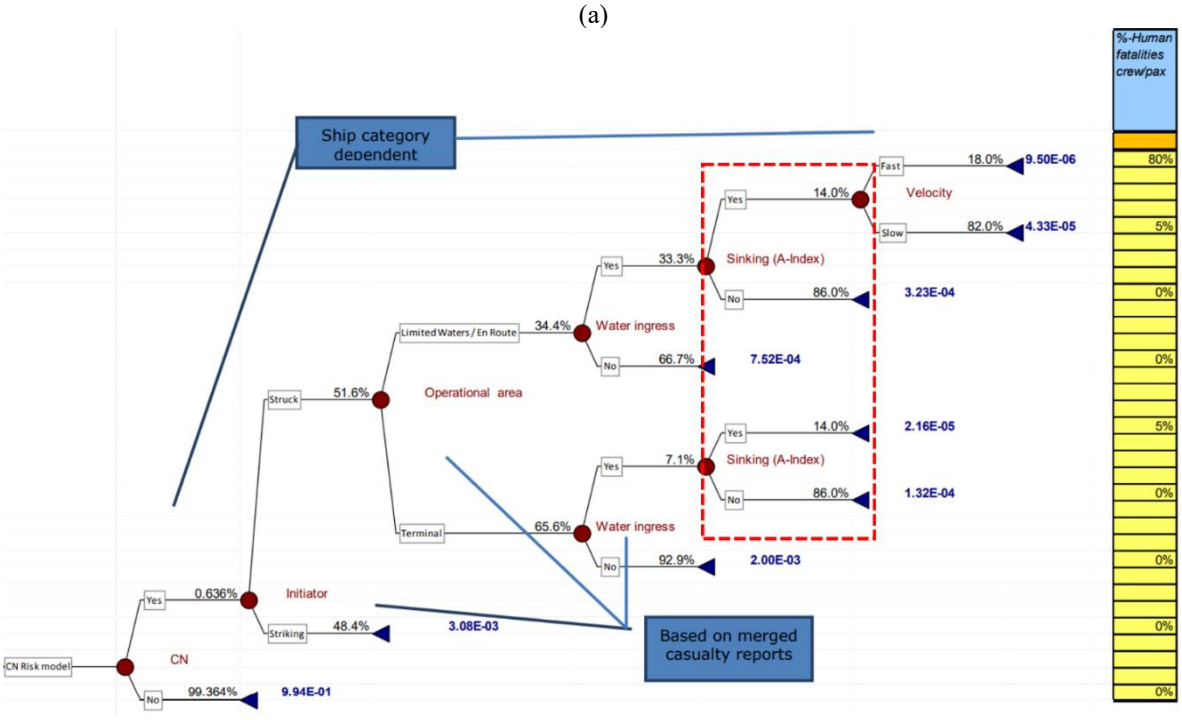

(b)

FigureB1: (a) High-level event sequences and (b) Collision risk model for cruise ships (EMSA, 2015)

C. Collision riks model

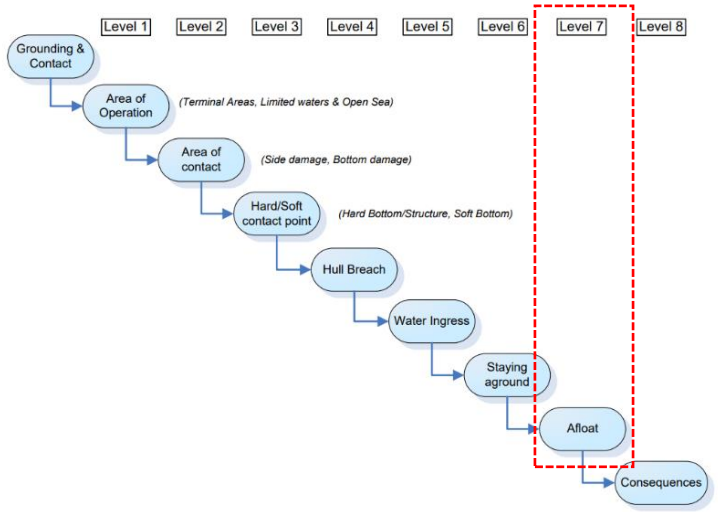

(a)

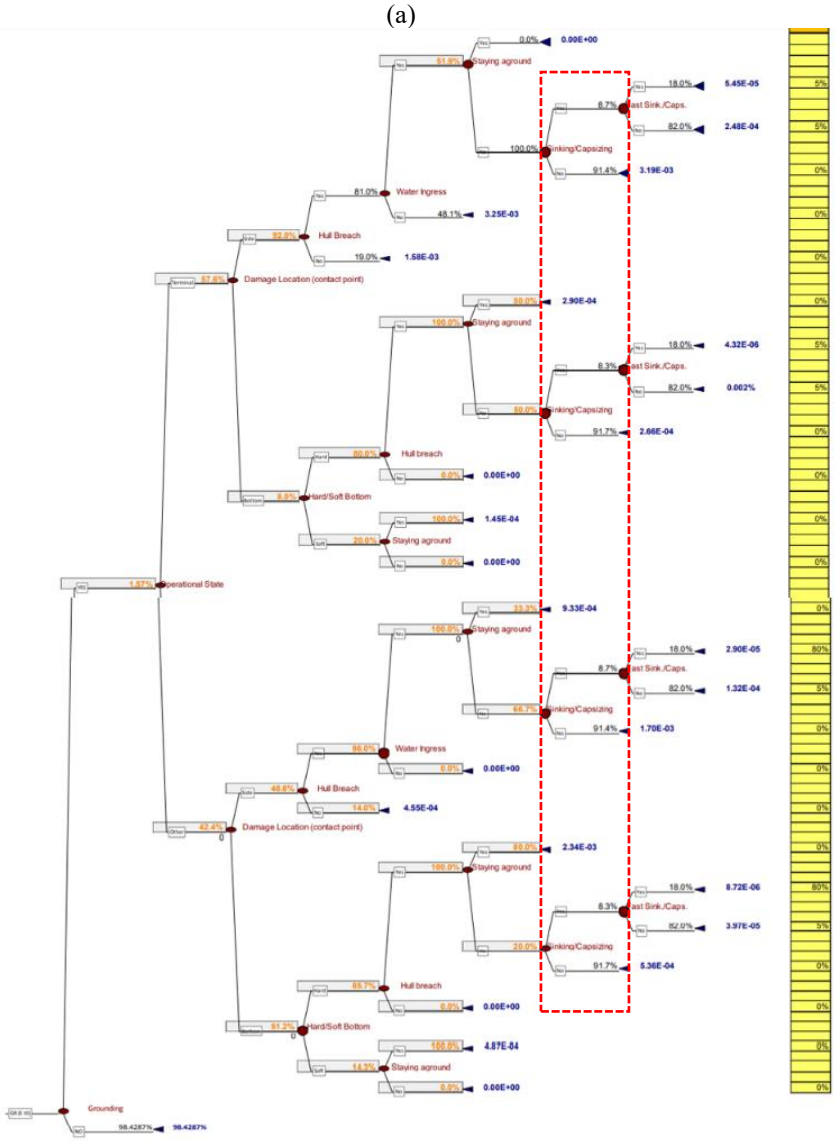

(b)

Figure C1: (a) High-level event sequences and (b) Grounding risk model for cruise ships (EMSA, 2015)